Polymer Journal, Vol. 24, No. 4, pp 311—321 (1992)

# Phase Equilibrium of a Three-Component System Consisting of Polystyrene, *N*,*N*-Dimethylformamide, and Cyclohexane

Yo NAKAMURA, Takayuki HIRAO, Yoshiyuki EINAGA,* and Akio TERAMOTO

*Department of Macromolecular Science, Osaka University, Toyonaka, Osaka 560, Japan*

(Received May 30, 1991)

ABSTRACT: Phase equilibrium and light scattering experiments were performed on a three-component system consisting of polystyrene (PS), *N*,*N*-dimethylformamide (DMF, good solvent), and cyclohexane (CH, poor solvent). The interaction function $\chi$ was expressed in the form proposed by Einaga *et al.*, *i.e.*, $\chi=\xi_1^2\chi_{11}^b(\phi_1)+\xi_2^2\chi_{22}^b(\phi_2)+2\xi_1\xi_2\chi_{12}^t(\phi_1,\phi_2)$, where $\chi_{11}^b$ is the interaction function for the binary system of DMF and CH, $\chi_{22}^b$, that for the binary system of PS and CH, and $\chi_{12}^t$ a function describing the interaction of PS and DMF in the presence of CH, with $\phi_1$ and $\phi_2$ denoting the volume fractions of DMF and PS in the system, respectively, and $\xi_i=\phi_i/(\phi_1+\phi_2)$ $(i=1,2)$. $\chi_{11}^b$ was determined by the Renon–Prausnitz theory along with cloud-point data, $\chi_{22}^b$ was calculated by the empirical equation of Einaga *et al.*, and $\chi_{12}^t$ was estimated from light scattering data using $\chi_{ii}^b$ $(i=1,2)$. With $\chi$ so obtained, binodals of the system at various temperatures on the triangular phase diagram were calculated and compared with those determined from cloud-point data. The agreement was only moderate. Reasons for this are discussed.

KEY WORDS Polystyrene / Phase Diagram / Light Scattering / Interaction Function / Ternary System / Thermodynamics /

Understanding of factors controlling phase equilibrium behavior of ternary polymer solutions has been of fundamental interest in polymer physical chemistry. Two cases have been the objects of investigation. In one, there are two monodisperse polymers, either chemically the same or different, in a pure solvent, and in the other, there is a monodisperse polymer in a mixture of two pure solvents. For the convenience of subsequent discussions, one solvent is chosen as component 0 and the rest (two polymers in the former; another solvent and one polymer in the latter) as components 1 and 2. With $i=1, 2$, we denote the volume fraction of component $i$ by $\phi_i$, and define $\xi_i$ by

$$\xi_i=\phi_i/\phi \qquad (\xi_1+\xi_2=1) \tag{1}$$

with $\phi=\phi_1+\phi_2$.

Usually, the chemical potential $\mu_0$ of component 0 is expressed in terms of the so-called $\chi$ function[1,2] as

$$(\mu_0-\mu_0^0)/RT=\ln(1-\phi)+(1-P_n^{-1})\phi+\chi\phi^2 \tag{2}$$

where $\mu_0^0$ is the chemical potential of pure 0, $R$ the gas constant, and $P_n$ is defined by $P_n^{-1}=\xi_1P_1^{-1}+\xi_2P_2^{-1}$ with $P_i=V_i/V_0$ and $V_i$ the molar volume of the component $i$ $(i=0, 1, 2)$. Recently, on the basis of some theoretical consideration, Einaga *et al.*[3] proposed the following expression for $\chi$:

$$\chi=\xi_1^2\chi_{11}^b(\phi_1)+\xi_2^2\chi_{22}^b(\phi_2)+2\xi_1\xi_2\chi_{12}^t(\phi_1,\phi_2) \tag{3}$$

Here, $\chi_{ii}^b(\phi_i)$ represents the $\chi$ function for the

* Present address: *Department of Polymer Chemistry, Kyoto University, Kyoto 606, Japan.*

binary system of component 0 and $i$, while $\chi_{12}^{t}(\phi_1, \phi_2)$ represents the interaction between components 1 and 2 in the ternary system lumping all the effects which the interaction between components 1 and 2 in the ternary system exerts on the chemical potential $\mu_0$. It should be noted that $\chi_{11}^{b}(\phi_1)$ and $\chi_{22}^{b}(\phi_2)$ can be determined from separate experiments on binary solutions.

For several systems consisting of two polymers and a single solvent, Tong *et al.*[4-6] estimated $\chi_{11}^{b}$, $\chi_{22}^{b}$, and $\chi_{12}^{t}$ from light scattering data, and found that the $\chi$ so obtained permitted fairly accurate predictions of experimentally observed phase relations.

This paper reports a similar study on a ternary system containing a monodisperse polystyrene (PS, component 2) in a mixed solvent made of cyclohexane (CH, component 0) and *N*,*N*-dimethylformamide (DMF, component 1). There were several facts that motivated our study. Firstly, the combination of PS, CH, and DMF is thermodynamically intriguing, because CH is a poor solvent and DMF is a good solvent for PS. Secondly, there were phase equilibrium studies on this system by Wolf and Willms[7] and Staikos and Dondos.[8] Thirdly, vapor pressure data allowing a test of $\chi_{11}^{b}$ (for CH+DMF) were available in the existing literature.[9] Fourthly, $\chi_{22}^{b}$ (for PS+CH) was also calculable by use of information accumulated at our laboratory.[10] It must be added that we abandoned the molecular theoretical standpoint of the Flory–Huggins theory by allowing the $\chi$ function to depend on composition as in eq 3.

## EXPERIMENTAL

### *Polymer Sample*

A Toyo Soda standard PS sample (F4) was used. Its weight-average molecular weight $M_w$, measured by light scattering on DMF solutions, was $5.10 \times 10^4$, and its $M_w/M_n$, estimated by GPC, was 1.05. Here, as usual, $M_n$ denotes the number-average molecular weight. The solvents cyclohexane and *N*,*N*-dimethylformamide used for physical measurements were fractionally distilled after being purified in the usual manner.

### *Cloud Point and Binodal*

Solutions for cloud point measurements were prepared in the following way. First, proper amounts of PS and CH were mixed at a desired ratio and dissolved in a stoppered flask. The solution was divided into several parts in measuring cells, and to each cell was added an appropriate amount of DMF, yielding a series of ternary solutions of the prescribed compositions of fixed PS/CH ratios. Proper amounts of DMF and CH were mixed directly to obtain DMF+CH mixtures. A test mixture in the cell was warmed at 50°C to become clear and uniform. Then it was cooled slowly with stirring, particularly at a rate slower than $0.1° \, min^{-1}$ near the cloud point. The cloud point was determined as the temperature at which light transmission across the solution decreased abruptly with lowering temperature.[11] The cloud point of a DMF+CH mixture was determined by visual inspection of the incipience of two phases. The binodal at a given temperature on the phase triangle was constructed from a series of cloud-point curves measured for solutions with different fixed values of PS/CH ratios.

### *Phase Separation*

Solutions for phase separation experiments were prepared by transferring a proper amount of a given PS+CH solution into a phase separation cell and diluting it with DMF and/or CH. The volume fractions $(\phi_1, \phi_2)$ of conjugated solutions at equilibrium were determined at 35 and 40°C in the following way. After made homogeneous at about 50°C, a test solution was cooled slowly under constant stirring to the desired temperature. After it was confirmed that the desired temperature was maintained within $\pm 0.02$°C, the solution was left standing until it separated into two

equilibrium phases. It took about one day for the equilibrium to reach. The two phases separately taken out of the vessel were weighed and freeze-dried, the residual polymer in each was weighed, and the weight fractions $w_2$ of PS in the two phases were determined. The weight fraction $w_1$ of component 1 in each phase was then determined from the point in the phase triangle (weight fraction-basis) at which the constant $w_2$ line for the phase intersected with the corresponding binodals constructed as above; there were two $w_1$ values but the one consistent with the observed volume ratios of the phases was taken as the desired one. The weight fractions were converted to the volume fractions by using the relation

$$\phi_i = v_i^0 w_i / \sum_{j=0}^{2} v_j^0 w_j \qquad (i=0, 1, 2) \qquad (4)$$

where $v_i^0$ denotes the specific volume of component $i$. We used literature values 0.9343, 1.0594, and 1.2922 $cm^3 g^{-1}$ for the specific volumes of PS,[12] DMF,[13] and CH,[14] respectively.

*Light Scattering*

A Fica-50 photogoniometer was used, with vertically polarized incident light of 436 nm wavelength. The intensity of scattered light was determined in the range of scattering angle from 30 to 150°.

Measurements on ternary solutions were made in two single-phase regions in the phase triangle, one near the CH apex and the other near the DMF apex (see Figure 1). In the following, the former region is referred to as CH-rich and the latter region, DMF-rich.

CH-rich solutions were prepared by diluting PS+DMF solutions of various $\xi_2$ with CH to values of $\phi$ ranging 0—0.1. The value of $\xi_2$ was varied in the range 0.094—0.901. On the other hand, DMF-rich solutions were prepared by adding known amounts of PS to CH+DMF solutions of various $\zeta$ $[=\phi_1/(\phi_0+\phi_1)]$ to values of $\phi_2$ ranging 0—0.20.

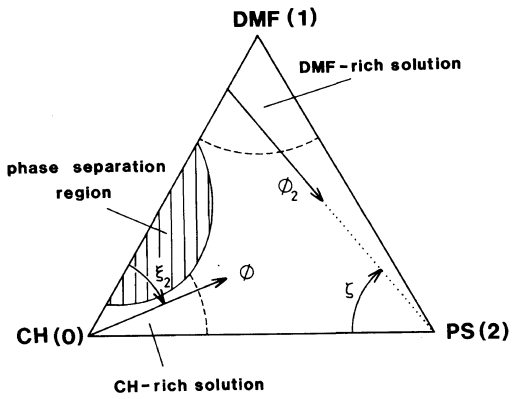


**Figure 1.** Schematic representation of a triangular phase diagram for the system PS+DMF+CH. Arrows, direction of dilution.

The value of $\zeta$ was varied from 0.756 to 0.948.

Measured intensities of scattered light had to be corrected for the contribution due to density fluctuation in order to extract the contribution due to concentration fluctuation. We made this correction for CH-rich solutions by subtracting the scattering intensity of pure CH and that for DMF-rich solutions by subtracting the scattering intensities of CH+DMF mixtures. The intensity ratio was 1 : 1.19 : 1.45 for pure CH : pure DMF : CH+DMF with $\zeta=0.75$, at 25°C and 436 nm wavelength. We note that intensity of a CH+DMF mixture contains the contributions from concentration fluctuation as well as density fluctuation.

The volume fraction-basis refractive index increment at low PS concentration is denoted by $\gamma_2$ for the PS+CH binary system and $\gamma_2'$ for the PS+DMF binary system. In the limit of vanishing $\phi_2$, $(\partial/\partial\phi_2) \simeq (\partial/\partial c_2)/v_2^0$, with $c_2$ denoting the mass concentration of PS. Using Cantow's data[14] for $\partial n/\partial c_2$, we obtained $\gamma_2 = 0.1011 + 3.10 \times 10^{-4} T$, where $n$ and $T$ are the refractive index of the system and the temperature in kelvins, respectively. For the PS+DMF binary system we measured $\partial n/\partial c_2$ and found $\gamma_2'$ to be 0.188 independent of temperature. We also measured the refractive index increment for the CH+DMF binary system at 25°C and found it to depend on

composition in a complex fashion, with a minimum value of $-0.026$. Thus, $\gamma_1$ defined as $(\partial n/\partial \phi_1)_{\phi_2=0}$ is much smaller than $\gamma_2$ and $\gamma_2'$, but may not be neglected.

All manipulations, solution preparation through transfer, were carried out in a dry bag filled with nitrogen gas and necessary precautions were taken in other operations to avoid humidity.

## RESULTS

### *Cloud Point Curves and Phase Diagram*

Figure 2 shows cloud point curves for the system PS + DMF + CH, where the cloud point temperature is plotted against the volume fraction $\phi_{DMF}$ $(=\phi_1)$ of DMF for a series of mixtures with different PS/CH ratios, the volume fraction of PS in PS + CH covering the range between 0 and 0.3496. The smooth solid and dashed curves represent the cloud point curves for the respective mixtures. Cloud point

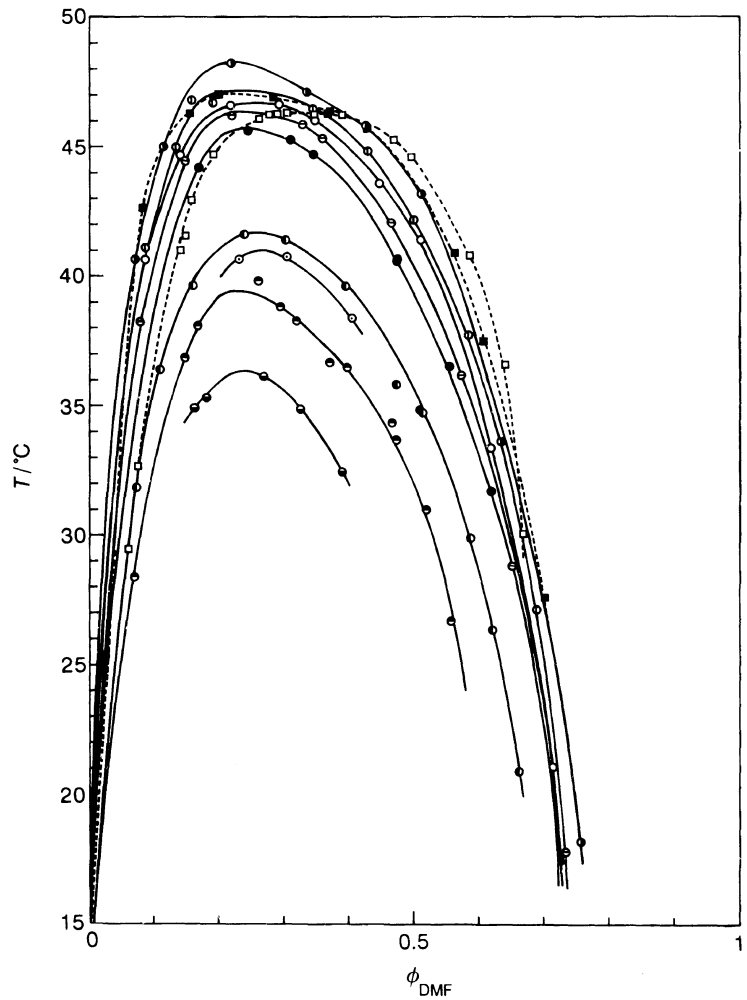


**Figure 2.** Cloud point curves for the system PS + DMF + CH with varying PS fractions in PS + CH mixture. $\phi_2/(\phi_0+\phi_2)$ values: ■, 0.0359; ◑, 0.0614; ◫, 0.08392; ○, 0.1092; ⊖, 0.1404; ●, 0.1649; ◐, 0.2376; ⊙, 0.2600; ◓, 0.2957; ◒, 0.3496. Unfilled squares, data for DMF + CH.

temperatures were determined for the PS + CH mixtures, at $\phi_{DMF} = 0$. They should be plotted on the ordinate axis in Figure 2, but are not shown for clarity. Each curve in the figure has been drawn to reach the respective point for the same PS/CH ratio on the ordinate axis. With increasing $\phi_2/(\phi_2+\phi_0)$, the upper solution temperature goes up and the cloud point curve tends to shift to lower $\phi_{DMF}$. Further increase in $\phi_2/(\phi_2+\phi_0)$ shifts the cloud point curve downward. These trends are in agreement with those found by Wolf and Willms[7] and consistent with the results of Staikos and Dondos.[8]

Figure 3 shows the binodals at different temperatures in the phase triangle. Here, $\phi_1$ and $\phi_2$ have been replaced by $\phi_{DMF}$ and $\phi_{PS}$, respectively, to facilitate the understanding of the diagram. The binodals at 47°C and 48°C are closed, while those at temperatures below 46°C intersect with the $\phi_{DMF}$ edge, as already observed by Wolf and Willms[7] in a PS ($M_w = 11 \times 10^4$) + CH + DMF ternary system. As the temperature is lowered, the two-phase domain expands, and the binodal nearly touches the $\phi_{PS}$ edge at 15°C, which is consistent with the previous finding that our PS + CH binary system has a critical temperature at about 14°C.[11]

Recently, Kawate *et al.*[15] investigated the phase behavior of a ternary system consisting of polystyrene, nitroethane, and cyclohexane. Although reported phase diagrams are similar to ours given in Figure 3, they have no closed binodals. This difference may be due to the fact that nitroethane is a poor solvent for PS,

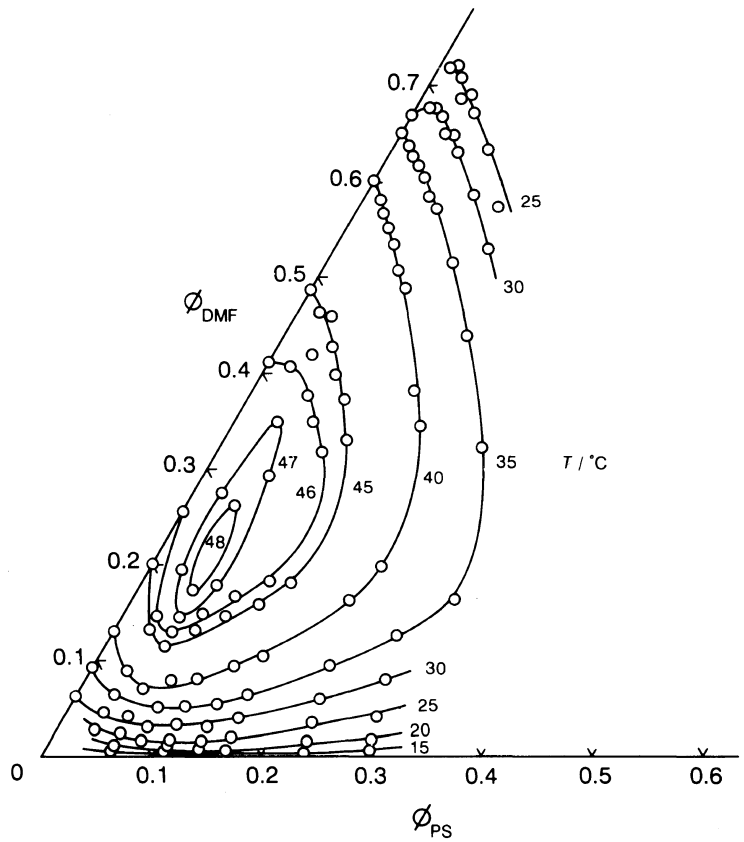


**Figure 3.** Triangular phase diagram for the system PS + DMF + CH. Circles connected by curves, binodals at the respective temperatures.

while DMF is a good solvent.

*Light Scattering Envelopes*

*PS+DMF System.* Figure 4 displays typical light scattering data for the PS+DMF binary system, shown as $KV_1\phi_2/\Delta R_0$ plotted against $\phi_2$. Here $V_1$ is the molar volume of DMF, $\Delta R_0$ the excess Rayleigh ratio extrapolated to zero scattering angle, and $K=4\pi^2n^2/(N_A\lambda_0^4)$ with $N_A$ and $\lambda_0$ being the Avogadro constant and the wavelength of the light *in vacuo*, respectively. Measurements at 15, 25, 35, and 45°C yielded essentially the same data, as expected from the fact that DMF is a good solvent for PS.

*PS+CH+DMF System.* Figure 5 displays the data obtained in the CH-rich region. Here, the relations between $KV_0\phi/\Delta R_0$ and $\phi$ at different $\xi_2$ are shown as a function of temperature, where $V_0$ denotes the molar volume of CH. It can be shown that the limiting value of $KV_0\phi/\Delta R_0$ at $\phi=0$ equals $[\gamma_1^2(1-\xi_2)P_1+\gamma_2^2\xi_2P_2]^{-1}$. Since, as mentioned above, $\gamma_1^2\ll\gamma_2^2$, and $P_1\ll P_2$ for our PS sample, we have with sufficient accuracy,

$$\lim_{\phi\to 0} KV_0\phi/\Delta R_0=(\gamma_2^2\xi_2P_2)^{-1} \qquad (5)$$

The points on the ordinate axis in Figure 5 were obtained by this equation. We see that, as expected, they are consistent with the values obtained by graphical extrapolation of the respective curves to zero $\phi$.

Figure 6 illustrates the data obtained in the DMF-rich region. Here, the relations between $KV_0\phi_2/\Delta R_0$ and $\phi_2$ at different $\zeta$ are shown as a function of temperature.

We note from these figures that the concentration dependence of the reduced scattering intensity is more complex in the CH-rich region than in the DMF-rich one and depends on temperature much less in the latter than in the former. In the Discussion section, we refer to the solid lines drawn in either figure, which are not eye-guides for the plotted points but have been calculated from the $\chi$ function derived.

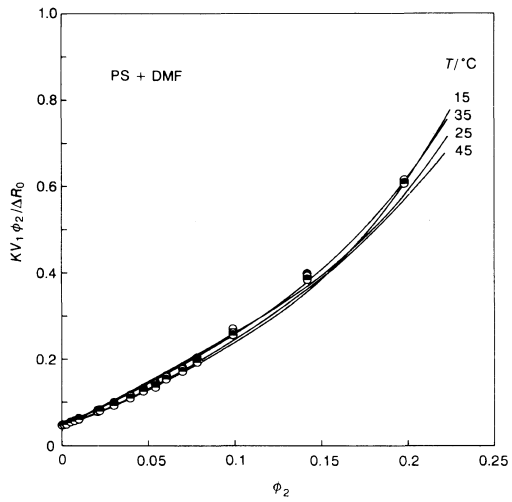


**Figure 4.** Light scattering data for the system PS+DMF. Circles, experimental values. Curves, calculated values.

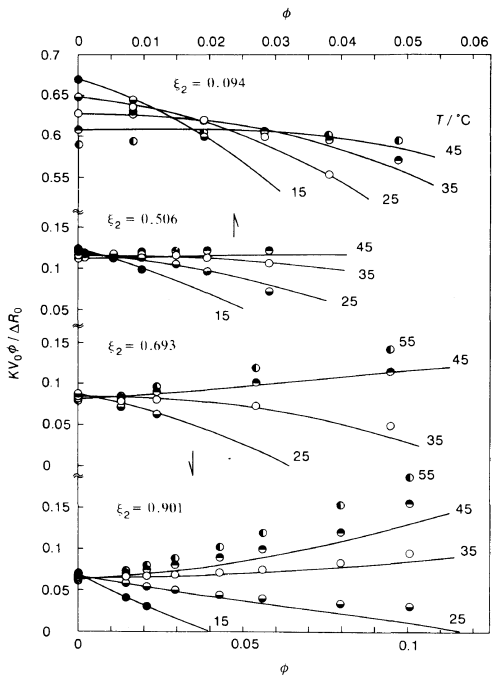


**Figure 5.** Light scattering data for the PS+DMF+CH with different fixed $\xi_2$ in the CH-rich region. ●, 15°C; ◒, 25°C; ○, 35°C; ◓, 45°C; ◐, 55°C. Curves, calculated values.

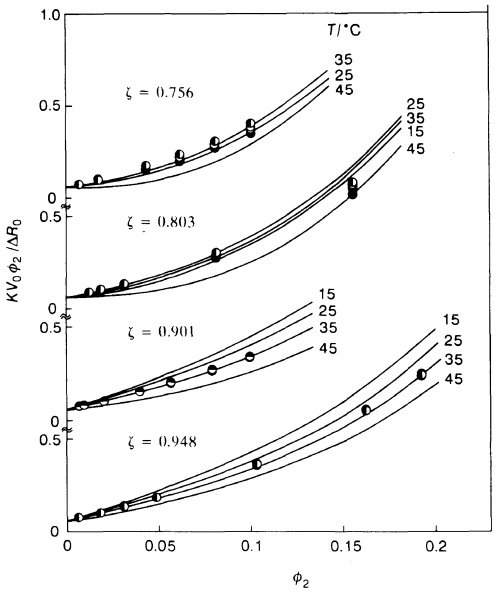


**Figure 6.** Light scattering data for the system PS+DMF+CH with different fixed $\zeta$ in the DMF-rich region at temperatures between 15 and 45°C. Symbols are the same as those in Figure 5. Curves, calculated values for the respective temperatures.

## DISCUSSION

*Interaction Function $\chi_{22}^b$ for PS+CH*

For the interaction function $\chi_{22}^b$ we use the empirical equation derived by Einaga *et al.*,[10] which reads

$$\chi_{22}^b(\phi_2)=(1/\phi_2^2)\int_0^{\phi_2} L_{22}(u)u\mathrm{d}u \tag{6}$$

where

$$L_{22}(u)=2[\chi_{conc}^0+u/2+Au^4/(1+Bu^2)+(\chi_{dil}^0-\chi_{conc}^0)R(uP_2^{1/2})] \tag{7}$$

with

$$\chi_{conc}^0=0.493+0.345(\theta/T-1)+(-0.075P_2^{-1/2}-45P_2^{-2}+0.007)\times\exp[-(40-520P_2^{-2/3})(\theta/T-1)] \tag{8}$$

$$\chi_{dil}^0=0.50+0.26(\theta/T-1)+4.6(\theta/T-1)^2 \tag{9}$$

$$A=1.4P_2^{1/3} \tag{10}$$

$$B=7P_2^{1/3}\exp[-18(\theta/T-1)] \tag{11}$$

and

$$R(x)=\exp(-x-0.3x^3) \tag{12}$$

Originally, these expressions were determined on the basis of light scattering data for $T$ below the $\theta$ point (34.5°C). However, in the present analysis, we apply it to the system at $T$ above $\theta$, though this operation may introduce some error.

*Interaction Function $\chi_{11}^b$ for DMF+CH*

The Renon-Prausnitz equations[16] for the chemical potentials $\mu_0$ and $\mu_1$ of small molecules 0 and 1 in their binary mixture are as follows:

$$(\mu_0-\mu_0^0)/RT=\ln(1-x_1)+x_1^2\{\tau_{10}U_1^2/[(1-x_1)+x_1U_1]^2+\tau_{01}U_0/[x_1+(1-x_1)U_0]^2\} \tag{13}$$

$$(\mu_1-\mu_1^0)/RT=\ln x_1+(1-x_1)^2\{\tau_{01}U_0^2/[x_1+(1-x_1)U_0]^2+\tau_{10}U_1/[(1-x_1)+x_1U_1]^2\} \tag{14}$$

where $\mu_1^0$ is the chemical potential of pure 1 and $x_1$ is the mole fraction of component 1, and $U_1$, $U_0$, $\tau_{10}$, and $\tau_{01}$ are functions of $T$, which are related by

$$U_1=\exp(-\alpha\tau_{10}),\quad U_0=\exp(-\alpha\tau_{01}) \tag{15}$$

where $\alpha$ is a constant, Geier *et al.*[9] used successfully these equations to describe their vapor pressure data for the system CH+DMF. We used the same equations to analyze the cloud point data for this system shown in Figure 7.

We set $\alpha$ equal to $-1$, according to Marina and Tassios,[17] who showed that this choice of $\alpha$ is adequate for vapor pressure data on many binary mixtures of small molecules. Then we determined $\tau_{10}$ and $\tau_{01}$ so that the binodal calculated from eq 13 and 14 would agree with the cloud-point data. The following empirical forms were found to give close agreement:

$$\tau_{10}=-1.02+601/T \tag{16}$$

$$\tau_{01}=1.417-187/T \tag{17}$$

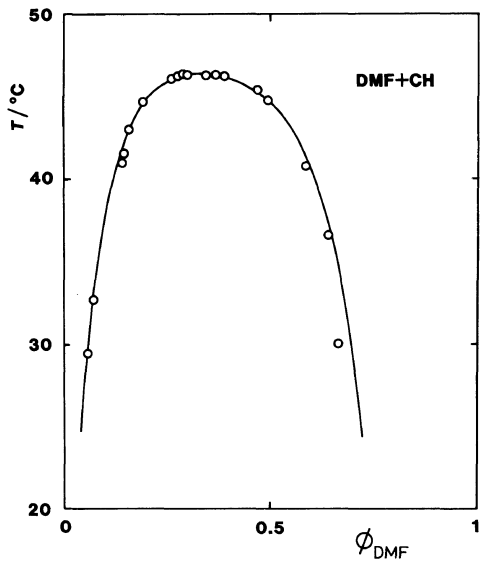


**Figure 7.** Comparison of the observed cloud-points with calculated binodal. Circles, cloud-points. Solid line, binodal.

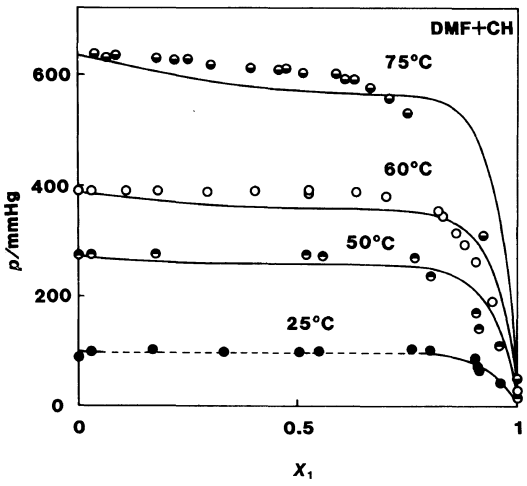


**Figure 8.** Vapor pressure of the system DMF+CH plotted against mole fraction $x_1$ of DMF at four temperatures. Circles, data of Geier *et al.*[9] Curves, calculated values.

The binodals calculated with these empirical forms are compared with the observed cloud-point data in Figure 7. The agreement is satisfactory except for one data point for the largest $\phi_{DMF}$.

Vapor pressures as a function of $T$ were calculated by eq 13—17 ($\alpha=-1$) along with the Antonie equation[13] for the vapor pressures of pure CH and DMF. The results (solid curves) are compared with the data of Geier *et al.*[9] in Figure 8. It can be seen that the agreement between the calculated and observed values is excellent at 25°C. The agreement is moderate at 50°C but not satisfactory at higher temperatures. However, this discrepancy has no serious effect on the discussion of the phase diagrams and light scattering data, because they are confined to temperatures below 45°C.

With the relation $\phi_1=P_1x_1/(P_1x_1+1-x_1)$, eq 13 gives

$$\chi_{11}^{b}(\phi_1)=(1/\phi_1^2)\ln\{P_1/[P_1(1-\phi_1)+\phi_1]\} -(1-P_1^{-1})/\phi_1 +\tau_{10}U_1^2/[P_1(1-\phi_1)+U_1\phi_1]^2 +\tau_{01}U_0/[P_1U_0(1-\phi_1)+\phi_1]^2 \quad (18)$$

We used this equation combined with eq 15—17 to calculate the interaction function for the CH+DMF binary system.

*Interaction Function $\chi_{12}^{t}$ for PS+CH+DMF*

*Basic Equations.* According to Tong *et al.*,[4] if the refractive index increments $\gamma_1$ and $\gamma_2$ are assumed to be composition-independent, the reduced excess intensity of scattered light for our ternary system can be represented by

$$KV_0\phi/\Delta R_0 \simeq [1+\phi(1-\phi)^{-1}P_w-\phi(P_wL+Y)]/WX \quad (19)$$

where

$$W=(\tilde{\gamma}_1^2P_1\xi_1+\tilde{\gamma}_2^2P_2\xi_2)/(1-\phi)^2 \quad (20)$$

$$X=1+(\tilde{\gamma}_1^2P_1\xi_1+\tilde{\gamma}_2^2P_2\xi_2)^{-1}\xi_1\xi_2 \times\{(\tilde{\gamma}_1-\tilde{\gamma}_2)^2P_1P_2[1+(P_n^{-1}-1)\phi]\phi -2(\tilde{\gamma}_1-\tilde{\gamma}_2)(\tilde{\gamma}_1P_1-\tilde{\gamma}_2P_2)\phi -(\tilde{\gamma}_1-\tilde{\gamma}_2)^2P_1P_2(1-\phi)^2\phi L +2(\tilde{\gamma}_1-\tilde{\gamma}_2)(\tilde{\gamma}_1\xi_1+\tilde{\gamma}_2\xi_2)P_1P_2(1-\phi)\phi M +(\tilde{\gamma}_1\xi_1+\tilde{\gamma}_2\xi_2)^2P_1P_2N\} \quad (21)$$

$$Y=\xi_1\xi_2\{2(P_1-P_2)M-P_1P_2[(1-\phi)^{-1}+(P_n\phi)^{-1}-L]N+P_1P_2\phi M^2\} \quad (22)$$

with

$$P_w=P_1\xi_1+P_2\xi_2 \quad (23)$$

$$L=2\chi+\phi(\partial\chi/\partial\phi)_{\xi_2} \quad (24)$$

$$M=(\partial\chi/\partial\xi_2)_\phi \quad (25)$$

$$N=-(\partial^2/\partial\xi_2^2)_\phi\int_0^\phi\chi(u,\xi_2)\mathrm{d}u \quad (26)$$

$$\tilde{\gamma}_i=\gamma_i-(\phi_1\gamma_1+\phi_2\gamma_2) \quad (27)$$

*Analysis on PS+DMF.* In the limit $\phi\to1$, eq 19 should give the equation for the PS+DMF binary system. The limiting form can be rewritten as

$$KV_1(\gamma_2-\gamma_1)^2/\Delta R_0=1/(1-\xi_2)+P_1/(P_2\xi_2)+P_1N(\phi=1) \quad (28)$$

Substituting eq 3 for $\chi$ into eq 26, with $\chi_{11}^b$ and $\chi_{22}^b$ given by eq 18 and eq 6, respectively, we obtain,

$$N(\phi=1)=(1-P_1^{-1})^2/[(P_1^{-1}-1)\xi_1-1]+2\tau_{10}(U_1/P_1)^2/[(1-U_1P_1^{-1})\xi_1-1]^3+2\tau_{01}(U_0/P_1)^2/[(U_0-P_1^{-1})\xi_1-U_0]^3-L_{22}(\xi_2)+H_{12}(\xi_2) \quad (29)$$

where

$$H_{12}(\xi_2)=-2(\partial^2/\partial\xi_2^2)\{\xi_2(1-\xi_2)\times\int_0^1\chi_{12}^t((1-\xi_2)\phi,\xi_2\phi)\mathrm{d}\phi\} \quad (30)$$

We calculated $N(\phi=1)$ from eq 28 with our light scattering data for the PS+DMF system in Figure 4 with the approximation $\gamma_2-\gamma_1=\gamma_2'$, and then $H_{12}(\xi_2)$ from eq 29 with eq 7 for $L_{22}(\xi_2)$. The results are illustrated by the circles in Figure 9. At any temperature indicated, the data points follow a declining curve somewhat bent upward, thus showing that $\chi_{12}^t(1-\xi_2,\xi_2)$ depends on $\xi_2$ more strongly than being linear.

For a curve-fitting operation we assume

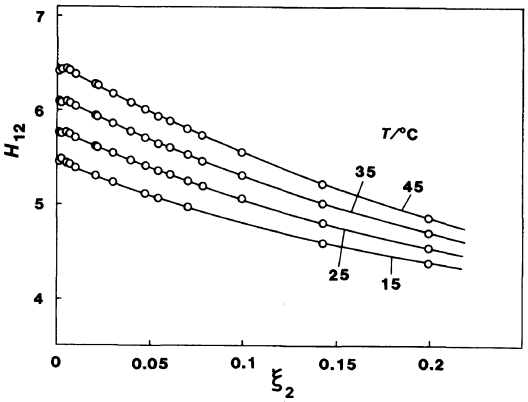


**Figure 9.** Values of $H_{12}$ for the system PS+DMF plotted against $\xi_2$ at four temperatures. Curves, calculated values.

for $\chi_{12}^t((1-\xi_2)\phi,\xi_2\phi)$ a general quadratic form as

$$\chi_{12}^t(\phi,\xi_2)\equiv x_{12}^t((1-\xi_2)\phi,\xi_2\phi)=k_0+[k_1\xi_2+k_2(1-\xi_2)]\phi+[k_3\xi_2^2+k_4\xi_2(1-\xi_2)+k_5(1-\xi_2)^2]\phi^2 \quad (31)$$

where the $k_i$ are functions of temperature. With eq 31 we obtain

$$H_{12}(\xi_2)=J_0+J_1\xi_2+J_2\xi_2^2 \quad (32)$$

where

$$J_0=2[2k_0-k_1+2k_2-(2/3)k_4+2k_5] \quad (33)$$

$$J_1=2(3k_1-3k_2-2k_3+4k_4-6k_5) \quad (34)$$

$$J_2=8(k_3-k_4+k_5) \quad (35)$$

We tried to determine $J_0$, $J_1$, and $J_2$ so that eq 32 fits the data of Figure 9 as closely as possible and obtained

$$J_0=0.0341T-4.37 \quad (36)$$

$$J_1=-0.094T+19.5 \quad (37)$$

$$J_2=0.0133T+7.3 \quad (38)$$

The solid curves in Figure 9 show the values of $H_{12}(\xi_2)$ computed with these expressions for the $J_i$. Once $H_{12}(\xi_2)$ is determined in this way, it is possible to calculate $N(\phi=1)$ from

eq 29 and then $KV_1\phi_2/\Delta R_0$ from eq 28. The results of calculation are shown by the solid lines in Figure 4 (note that $\phi_2=\xi_2$ at $\phi=1$).

*Analysis of Scattering Data for PS+CH+DMF.* Solving eq 33—35 for $k_3$, $k_4$, and $k_5$, we obtain

$$k_3=(1/8)(6J_0+4J_1+3J_2-24k_0-12k_1) \quad (39)$$

$$k_4=(3/8)(4J_0+2J_1+J_2-16k_0-4k_1-4k_2) \quad (40)$$

$$k_5=(1/8)(6J_0+2J_1+J_2-24k_0-12k_2) \quad (41)$$

Thus, once $k_0$, $k_1$, and $k_2$ are determined, the six unknown coefficients in eq 31 and hence $\chi_{12}^t$ can be estimated.

We evaluated $k_0$, $k_1$, and $k_2$ by applying a trial and error method to our light scattering data on the system PS+DMF+CH, and obtained

$$k_0=0.02T-5.25 \quad (42)$$

$$k_1=-0.068T+21.67 \quad (43)$$

$$k_2=-0.091T+27.1 \quad (44)$$

The calculated scattered intensities for CH-rich and DMF-rich solutions gave the solid lines in Figure 5 and Figure 6, respectively. These lines fit the experimental points only semi-quantitatively. Especially, in Figure 6, they show distinct temperature dependence for all values of $\zeta$ examined, while the data points show no such behavior. This is due to

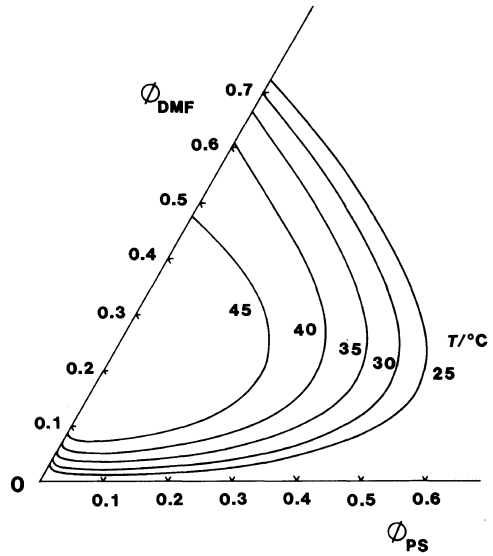


**Figure 10.** Calculated binodals for the system PS+DMF+CH at various temperatures.

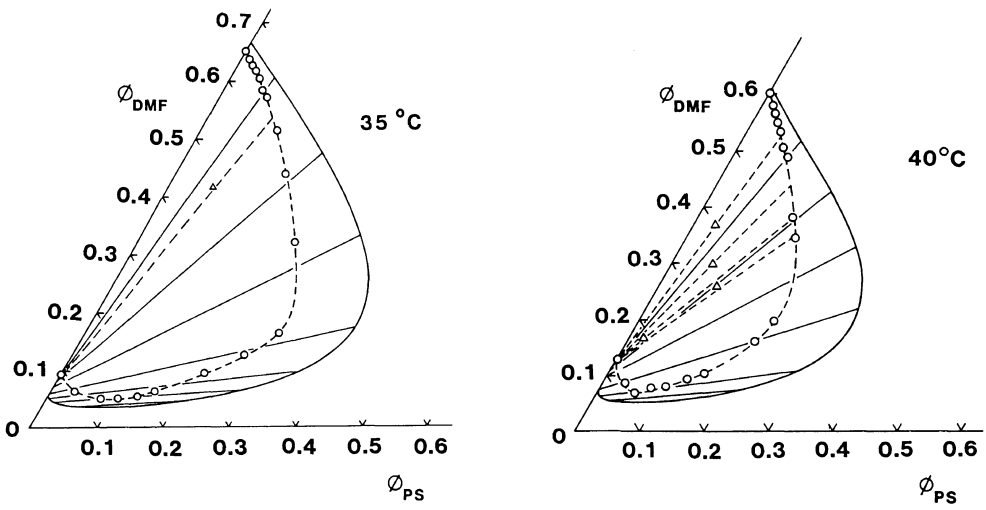


**Figure 11.** Comparison of observed and calculated binodals and tie lines for the system PS+DMF+CH at 35 and 40°C. Circles connected by dashed curves, observed binodals; straight dashed lines, observed tie lines; triangles, compositions of the solution before phase separation; solid curves, calculated binodals; solid straight lines, calculated tie lines.

approximating $\chi_{12}^{t}$ by a polynomial quadratic in $\phi_1$ and $\phi_2$ and assuming the coefficients $k_0 \cdots k_5$ to depend linearly on $T$.

*Calculated Phase Diagrams*

Figure 10 shows the binodals calculated from the expression so determined for $\chi$. All intersect with the $\phi_{DMF}$ axis and the area enclosed by each of them gets narrower as the temperature is raised. Although not shown in the figure, closed binodals appear at temperatures above 47°C. These calculated binodals may be compared with experimental ones shown in Figure 3. In Figure 11, the calculated binodals and tie lines at 35 and 40°C are compared with the corresponding experimental data. It is seen that the calculated and experimental results are in good agreement for the direction of the tie line as well as the overall shape and position of the binodal. Indeed each binodal is terminated on the $\phi_{DMF}$ axis at positions close to the cloud points of the system DMF+CH. However, in comparison with the experimental data, the calculated phase separation region at relatively low polymer concentration expands toward lower $\phi_{DMF}$ and that at relatively high polymer concentration, toward $\phi_{PS}$. These disagreements are due to the inaccuracy in $\chi_{12}^{t}$.

## CONCLUSIONS

We determined the function $\chi_{12}^{t}$ in eq 3 for the system PS+DMF+CH by light scattering measurement, with the functions $\chi_{11}^{b}$ and $\chi_{22}^{b}$ for the binary solutions DMF+CH and PS+CH, respectively, estimated from available data. The resulting expression for $\chi$, however, predicted binodals which agreed only semi-quantitatively with measured ones. It exemplifies the well-known fact that phase relationships of multicomponent systems are very sensitive to the dependence of $\chi$ on the composition and temperature.

*Acknowledgment.* We are very grateful to Professor Emeritus Hiroshi Fujita of Osaka University for valuable comments on this manuscript.

## REFERENCES

1. P. J. Flory, "Principle of Polymer Chemistry," Cornell University Press, Ithaca, New York, 1953.
2. R. Koningsveld, H. A. G. Chermin, and M. Gordon, *Proc. R. Soc. London, Ser. A*, **319**, 331 (1970).
3. Y. Einaga, Z. Tong, and H. Fujita, *Macromolecules*, **20**, 2027 (1987).
4. Z. Tong, Y. Einaga, H. Miyashita, and H. Fujita, *Macromolecules*, **20**, 1883 (1987).
5. Z. Tong, Y. Einaga, and H. Fujita, *Polym. J.*, **19**, 965 (1987).
6. Z. Tong, Y. Einaga, T. Kitagawa, and H. Fujita, *Macromolecules*, **22**, 450 (1989).
7. B. A. Wolf and M. M. Willms, *Makromol. Chem.*, **179**, 2265 (1978).
8. G. Staikos and A. Dondos, *Polymer*, **26**, 293 (1985).
9. K. Geier, Chr. Mölke, and H.-J. Bittrich, *Z. Phys. Chem. (Leipzig)*, **262**, 491 (1981).
10. Y. Einaga, S. Ohashi, Z. Tong, and H. Fujita, *Macromolecules*, **17**, 527 (1984).
11. M. Tsuyumoto, Y. Einaga, and H. Fujita, *Polym. J.*, **16**, 229 (1984).
12. H. Höcker, G. J. Blake, and P. J. Flory, *Trans. Faraday Soc.*, **67**, 2251 (1971).
13. J. A. Riddick and W. B. Bunger, "Organic Solvents," Wiley-Interscience, New York, N.Y., 1970.
14. H.-J. Cantow, *Z. Physik. Chem. (Frankf.)*, **7**, 58 (1956).
15. K. Kawate, I. Imagawa, and M. Nakata, *Polym. J.*, **23**, 233 (1991).
16. H. Renon and J. M. Prausnitz, *AIChE J.*, **14**, 135 (1968).
17. J. M. Marina and D. P. Tassios, *Ind. Eng. Chem. Process Des. Develop.*, **12**, 67 (1973).